Identification of anisotropic tensile strength of cortical bone using Brazilian test

Rachele Allena[a,*], Christophe Cluzel[a,b,c]

[a] *Arts et Métiers ParisTech, LBM, 151 Boulevard de l'hôpital, 75013, Paris France*
[b] *LMT-Cachan, 61 av. du Président Wilson, 94235 Cachan France*
[c] *IUT-SGM, rue du PJarlan, 91025 Evry France*

Abstract

For a proper analysis of cortical bone behaviour, it is essential to take into account both the elastic stiffness and the failure criteria. While ultrasound methods allow complete identification of the elastic orthotropic coefficients, tests used to characterise the various failure mechanisms and to identify the brittle tensile strength in all directions are currently inadequate. In the present work we propose the Brazilian test as a complement to conventional tensile tests. In fact, this experimental technique, rarely employed in the biomechanics field, has the potential to provide an accurate description of the anisotropic strength of cortical bone. Additionally, it allows to assess the scale influence on failure behaviour which may be attributed to an intrinsic length in correlation with the cortical bone microstructure. In order to correctly set up the Brazilian test, several aspects such as the machining, the geometrical parameters of the specimen and the loading conditions were determined. The finite element method was used to evaluate the maximal

*Corresponding author. Tel: +33 (0)1 44 24 61 18; Fax: +33 (0)1 44 24 63 66
Email address: rachele.allena@ensam.eu (Rachele Allena)

tensile stress at the centre of a 2D anisotropic elastic specimen as a simple function of the loading. To validate the protocol, the Brazilian test was carried out on 29 cortical bovine cylindrical specimens with diameters ranging from 10 mm to 4 mm.

Keywords: Cortical bone, Anisotropy, Brazilian test, Brittle strength

1. Introduction

1.1. Bone's structure and behaviour

Bone presents a hierarchical structure (Currey, 2001) (Rho et al., 1998) (Vashishth, 2007) which is organised in different levels as follows: i) the macrostructure: cancellous and cortical bone, ii) the mesostructure (from 10 to 500 μm): haversian system, osteons, trabeculae and iii) the microstructure (1-10 μm): the lamellae and the osteocytes iv) the nanostructure (from a few hundred nanometers to 1 μm): fibrillar collagen and embedded mineral v) the sub-nanostructure (below a few hundred nanometers): collagen, molecules and proteins.

The complex structure of the bone has been the object of many studies during the last decades in order to decipher the influence of each level on both the mechanical and failure behaviour (Currey, 2001) . At the nanoscale, the orientation of the collagen fibrils and their degree of mineralisation (Turner-Walker and Parry, 1995) may affect the Young's modulus leading to a failure stress in the fibres direction. At the microscale, the stacking of successive lamellae, each composed by collagen fibres oriented in a single direction, provides an isotropic mechanical behaviour in the lamellae plan, while weak properties are observed along the perpendicular direction. At the mesoscale,

the osteons structure supplies a transverse isotropy for both the stiffness and the failure stresses (Rho et al., 1998) (Ascenzi et al., 2012). Such a behaviour is maintained at the macroscale due to the main orientation of the osteons along the longitudinal axis of the bone. Finally, at this level the interface between the osteons and the interstitial lamellae (the cement line) brings a further weakness to the failure behaviour.

Conventional mechanical tests in traction, compression and torsion on specimens obtained from cortical bone of the femur diaphysis were carried out by Reilly and Burstein (1975). They actually observed that the Young's modulus along the longitudinal direction is double that measured along the circumferential or radial directions. Therefore, the anisotropy of the elastic behaviour is clearly marked and complies with the geometrical organisation of the bone at the mesoscopic scale.

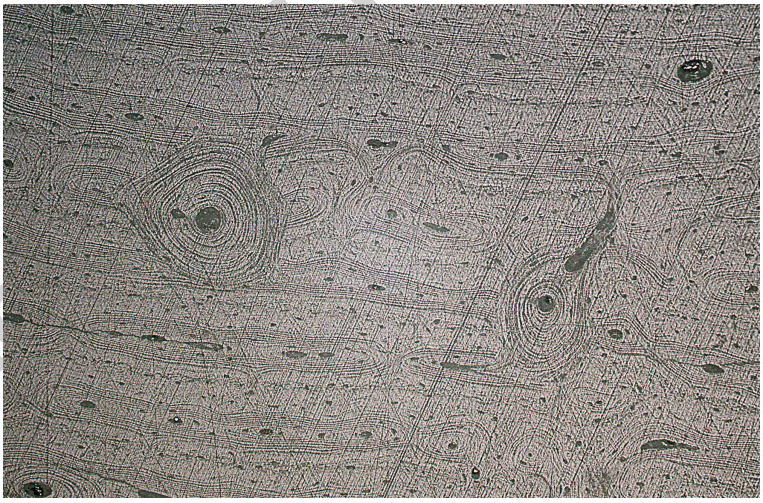

Figure 1: Bovine bone microstructure: sections perpendicular to the longitudinal axis

Nevertheless, this anisotropy is not limited to stiffness, it also influences

failure behaviour. As has been pointed out in (Norman and Wang, 1997) (O'Brien et al., 2007) (MFeerick et al., 2013), the cement line is a source of weakness that may enhance crack propagation. Similarly, the interface between two lamellae may reduce the failure threshold along their perpendicular direction when several of them are aligned in a circumferential direction as it is shown in Fig. 1 for cortical bone of a young bovine. In contrast, along the longitudinal direction, the lamellae and the osteons are continuous and, for longitudinal loading, rupture occurs with a very high stress. In parallel to the analysis of failure mechanisms, many studies have focused on the failure criterion and have shown that taking into account the failure anisotropy allows better predictive ability (Doblare et al., 2004). Nonetheless, these criteria are very complex to identify experimentally. Additionally, Hashin (1996) and Puck and Schürmann (1998) for fibre reinforced plastic (FRP) composite and Arramon et al. (2000) for bone have pointed out that a multicriterion approach in which each function is related to a specific failure mechanism is more suitable than a quadratic function defining an admissible rupture domain. Therefore, it is essential to identify the failure mechanism in order to determine which stress triggers the rupture.

1.2. Mechanical tests

During mechanical tests on brittle material, two different sets of parameters can be measured: i) those describing the elastic behaviour and ii) those describing the failure thresholds for each loading condition.

In order to identify the orthotropic elastic coefficients of cortical bone, it is first necessary to perform traction or compression tests in the three main directions as presented in Reilly and Burstein (1975) for a bovine femoral

cortical bone. Secondly, the shear elastic behaviour may be assessed through Iosipescu or Arcan tests as described in Xavier et al. (2013), or by torsion tests like those employed by Reilly and Burstein (1975). Nonetheless, the ultrasonic method presented in Rho et al. (1998) on bovine cortical bone and the nano indentation used in Hoc et al. (2006) and Vayron et al. (2012) may be very useful for a complete identification of the elastic parameters and for studying the spatial variations of the modulus, respectively. Additionally, resonant ultrasonic spectroscopy techniques (Bernard et al., 2013) have been recently employed for both human and bovine cortical bone and have confirmed the previous results with high accuracy. For bovine cortical bone, the values of Young′s moduli along the circumferential and transverse directions are of the order of 12.8 GPa, while the Young′s modulus along the longitudinal direction is about 20.3 GPa.

Several experimental tests may be used to evaluate the strength for a brittle and anisotropic material like bone. Tensile testing is one of the classical methods to measure bone's mechanical properties. Nevertheless, specimens must have relatively large dimensions (15-20 mm in length, 4-8 mm in width) and they must be specifically designed to obtain the majority of the strain in the central region (Reilly and Burnstein, 1974) (Ashman et al., 1987). If one assumes that the external force is applied without inducing a bending moment, the tensile test provides a good assessment of bone's strength, but is limited in its ability to evaluate the effects of anisotropy due to the constraints on the dimensions of specimens.

Bending tests are usually employed for testing the bones of small animals, for which a tensile test is difficult to set up. In such a test, the entire

bone is loaded until failure leading to tensile stresses on one side of the bone and compressive stresses on the other side. Additionally, tensile or compressive stresses increase from the neutral axis to the external boundaries of the specimen. Thus, failure commonly occurs on the tensile side since bone is weaker in tension than in compression (Reilly and Burstein, 1975) and may also be highly sensitive to surface defects due to the machining of the specimens for instance. Bending may be applied to the bone through either a three-point or a four-point loading. The former is very simple to set up, but it may cause high shear stress around the middle section of the bone. The latter induces pure bending and ensures zero transverse shear stress between the two upper loading points. Nevertheless, if the specimen is rather small in length and the bending moment is maximum under the loading point, the stress state is not easy to determine. Furthermore, in both three-point and four-point bending tests the total length of the specimen should be about sixteen times the thickness of the specimen to guarantee that 85-90 % of the bone flexion is actually due to bending. Unfortunately, this length-width ratio cannot be acquired in whole bones such as femora or tibias.

For compression testing, relatively small specimens (7-10 mm long) can be used and therefore machined along the three directions, but the measurement tends to be less accurate than those for tensile tests because of edge effects. In those regions in fact, the strain is likely to be higher than in the central region, possibly due to the misalignment of the specimen faces or other problems associated with specimen machining. Then, because of friction between the contact surfaces of the bone specimen and the plates of the testing machine, one may have a unidirectional strain at the boundaries and a stress static

state in the central region, such that the specimen acquires a barrel-like shape. Although an extensometer is usually employed during tensile tests to determine the axial strain in the specimen, this is not possible in compression due to the small dimensions of the specimen. In this case image correlation represents an alternative method to evaluate the stress-strain relationship. Despite a lower accuracy of the results compared to tensile tests, compressive testing presents some major advantages. First, specimens do not have to be as large as tensile specimens. Second, machining of compressive specimens is easier than for tensile specimens and may be done in different directions to investigate the anisotropic behaviour of the bone. Nevertheless, compression tests do not initiate the same failure modes as tensile tests (for which failure mode and crack shape show a specific brittle mechanism).

In recent years, shear tests have been developed to determine the shear modulus of elasticity of the bone. Among them we mention the rail shear test, the torsion tube, cross-beam specimens and tension-compression of notched specimens, including the Iosipescu (ASTM D5379) (Iosipescu, 1967) (Funk and Litsky, 1998) (Sharma et al., 2011) and the Arcan tests (Arcan et al., 1978).

Although the previous resistance tests allow partial assessment of the anisotropic characteristics of cortical bone's behaviour and identification of some fracture modes, they fail in evaluating the anisotropy in traction. For this reason, here we propose the Brazilian test as an alternative experimental approach to characterise the bone failure responses along the longitudinal, circumferential and radial axes. Such a test presents interesting features, which appear to be decidedly appropriate to study bone's mechanical be-

haviour and to obtain a complete predictive model.

1.3. Brazilian test for brittle materials

The Brazilian test was first introduced by Carneiro (1943) and Akazawa (1943) to determine the tensile strength of brittle materials such as rock, concrete or ceramic, which is difficult to evaluate by performing a direct uniaxial tensile test. It is widely used in the field of civil engineering and has been the object of numerous works for both the calculation of stresses and the identification of material properties (Li et al., 2013). In the biomechanics field, it has been employed to determine the tensile strength of archeological cortical bone (Turner-Walker and Parry, 1995) and artificially aged bone (Turner-Walker, 2011). Additionally, (Huang et al., 2012) proposed a numerical analysis of the Brazilian test of heterogeneous specimens in order to analyse the tensile strength of dental amalgams.

In the Brazilian test, a cylindrical specimen is loaded in compression until failure over a short strip along the specimen length at each end of the vertical diameter. Compression induces tensile stresses normal to the loading direction, which are approximately constant within a region around the centre. Therefore, for a brittle material, a crack appears perpendicular to the maximum traction stress direction, leading to the splitting of the cylinder into two halves.

The Brazilian test has some interesting characteristics. Firstly, it greatly simplifies the traction loading of a brittle material. Secondly, it permits reduction of the size of the specimen down to that limited by testing a representative volume of the material. For the specific case of cortical bone, such a reduction in dimensions (e.g. some millimetres in diameter) leads to

three further benefits: i) it decreases the probability of finding very large defects that may induce macroscopic rupture, ii) it provides information on the correlation between specimen size and defect distribution and iii) it enables the analysis of the traction fracture along the three main axes of the bone. Therefore, the Brazilian test may be employed to provide an accurate identification of the anisotropic maximal traction stresses in cortical bone.

2. Materials and methods

2.1. Sample preparation

Specimens were obtained from a bovine tibia sourced from a local butcher and conserved at $-18°$. Once the tibia was defrosted, the internal marrow and spongy bone were removed and the bone was cleaned with water. The three main local axes of the bone were chosen as follows (Fig. 2):

- the longitudinal axis x_1 corresponds to the main direction of the tibia;
- the circumferential axis x_2 coincides with the azimuthal direction;
- the radial axis x_3 is aligned with the outward radius of the bone's section.

First, 25 bone cylinders were machined using diamond-tipped tubular drills of internal diameters ϕ 10, 8, 6 and 4 mm. For the sake of convenience, the machining was performed along the x_1 and x_3 directions, which maintains the ability to obtain the three fracture stresses σ_{11}^f, σ_{22}^f and σ_{33}^f ((Fig. 2), the superscript f indicates failure). Second, the cylinders were sectioned perpendicular to the cylinder axis using a diamond disc saw. Furthermore, for

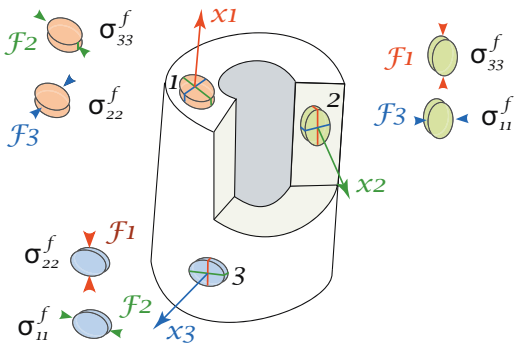

Figure 2: Coordinates system, traction stresses (σ_{ii}^f) and loading directions (F_j).

those machined along the x_1 direction, more than one specimen was obtained. Finally, 29 specimens were acquired. The length L of the samples was set to 6.5 mm, 5.2 mm, 3.9 mm and 2.6 mm respectively for $\phi = 10$ mm, $\phi = 8$ mm, $\phi = 6$ mm and $\phi = 4$ mm (Fig. 3). Such values provide a minimal average ratio ϕ/L equal to 1.54. Before sectioning, the three main axes x_1, x_2 and x_3 were identified on each specimen which allows to classify the specimens as follows: $x_i\_F_j$, with x_i and F_j indicating the cutting axis and the loading direction, respectively (Fig. 2). During cutting, water was used in order to reduce both friction and temperature rise.

2.2. Brazilian test for cortical bone

The Brazilian tests were performed at room temperature right after the cutting, using a universal traction-compression machine INSTRON 5500-R equipped with a 5 KN sensor. We have assumed that the room humidity does not influence the specimens behaviour. The machine was controlled by fixing the displacement rate of the upper plate at 0.2 mm/min. The positioning of the specimen between the two plates of the machine as shown in Fig. 4 must

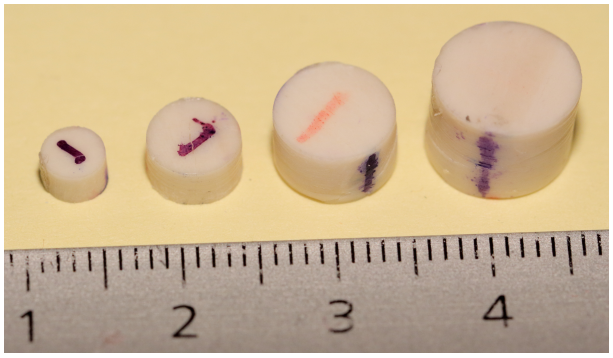

Figure 3: Specimens diameters: 4, 6, 8 and 10 mm.

be done very carefully since it was necessary i) to align the cylinder with respect to the mid-planes of the plates, ii) to orient the cylinder along the main axis of the machine and iii) to place the cylinder in the central region of the lower plate. Such conditions may not been verified if, for instance, there exists a parallelism or a cylindricality defect of the specimen, which may influence the stress distribution.

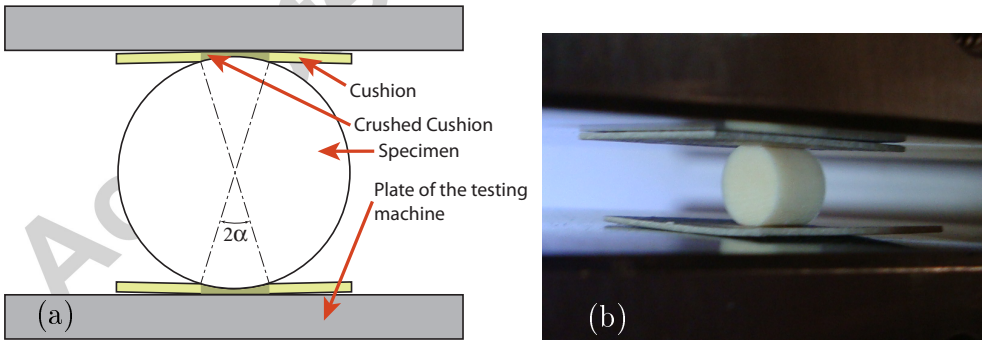

Figure 4: Schematic drawing of the Brazilian test (a) and positioning of a 4 mm diameter specimen (b).

During a regular test, the crack was generally initiated at the centre of

the cylinder along the vertical axis (Fig. 5). Nevertheless, abnormal splitting might be observed due to i) shear stress (Fig. 6a), ii) crushing issues (Fig. 6b) or iii) a non centred crack. Defects such as those presented in Fig. 6a were mainly found during a preliminary series of tests with specimens having a ratio $\phi/L < 1.54$. To limit the crushing of the contact surface (Fig. 6b), a cushion can be inserted between the specimen and each load plate as described in the standard for Brazilian tests applied to rocks (ISRM 1978, ASTM 2008). In our case, a 0.52 mm thick square of cardboard was used (Fig. 4). The imprint was measured after each test to estimate the contact area and we found that it can actually be defined independently of the specimen diameter ϕ through the angle α (Fig. 4a) as described in Wang et al. (2004).

2.3. Structural analysis of Brazilian test for anisotropic elastic behaviour

Through a structural analysis, we may be able to evaluate the maximal tensile stress $\sigma_{xx,max}$ along the x direction at the centre of each specimen. For isotropic materials, an analytical solution was proposed by Peltier (1954) giving the tensile stress in the centre of the disc as follows

$$\sigma_{xx,max} = \frac{2F}{\phi L \pi} \tag{1}$$

where F is the applied load.

To account for the effect of a soft cushion between the specimen and the loading plates, a factor of correction k was introduced by Hondros (1959) and Wang et al. (2004) as a function of the angle α (Fig. 7). Thus, Eq. [1] becomes :

Figure 5: Appearance of a vertical crack at the centre of a specimen $x_1\_F_3$ with a 8.12 mm diameter.

$$\sigma_{xx,max} = k(\alpha)\frac{2F}{\phi L\pi} \tag{2}$$

Nonetheless, the previous relation is no longer valid for an anisotropic elastic behaviour as for the cortical bone. In Exadaktylos and Kaklis (2001), the authors propose an analytical approach in the form of a sum of Fourier series, which is validated for the isotropic case by comparing it with the results of Hondros (1959). In the present work, in order to have an extensive

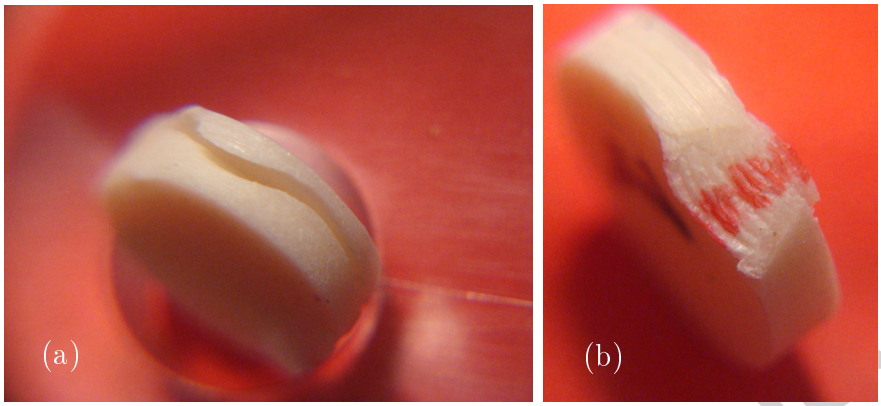

Figure 6: Examples of abnormal splitting due to shear stress (a) and matting (b).

overview of anisotropy effects, the definition of the maximum tensile stresses (Fig. 2) is similar to that proposed in Eq. [2], but the coefficient of correction is now expressed as a function of both the direction of the failure stress and of the loading. Thus, we have:

$$\sigma_{ii,max} = \beta_{ii-j} \frac{2F_j}{\phi L \pi} \tag{3}$$

where β_{ii-j} is the correction factor and F_j is the applied vertical load. The subscripts ii and j indicate the principal stresses and loading direction, respectively. The main objective of the structural analysis is to find the coefficient β_{ii-j} for the different directions independently of the specimen diameter ϕ.

In the present study, the analysis was performed using the finite elements (FE) method, which provides a better validation and simplify the management of various input and output data. The FE software COMSOL 3.5a was used to run two dimensional (2D) simulations and to evaluate the linear

elastic stress field within the samples along x_1, x_2 and x_3 with two loading directions each. The cylindrical specimens were represented as circles with an anisotropic elastic behaviour. The elastic material parameters were deduced from Bernard et al. (2013) (Table 1).

Modulus	Value	Reference or formula
E_1	20.3 GPa	(Bernard et al., 2013)
E_2	12.8 GPa	(Bernard et al., 2013)
E_3	12.8 GPa	(Bernard et al., 2013)
G_{12}	6.38 GPa	(Bernard et al., 2013)
G_{13}	6.32 GPa	(Bernard et al., 2013)
G_{23}	6.38 GPa	(Bernard et al., 2013)
ν_{12}	0.421	(Bernard et al., 2013)
ν_{13}	0.434	(Bernard et al., 2013)
ν_{23}	0.348	(Bernard et al., 2013)
ν_{21}	0.265	$\frac{\nu_{12}E_2}{E_1}$
ν_{31}	0.273	$\frac{\nu_{13}E_3}{E_1}$
ν_{32}	0.348	$\frac{\nu_{23}E_3}{E_2}$

Table 1: Elastic parameters sourced and deduced from Bernard et al. (2013).

The problem was solved using the plane stress hypothesis. The displacement of the point A was constrained along the x direction while the point B was totally constrained to prevent rigid body motion (Fig. 7). Finally, the vertical load was applied along the upper and lower boundaries l (blue lines in Fig. 7), which, as previously explained (Sec. 2.2), have been calculated

using the angle $\alpha = 14°$. Thus, l is equal to 2.4 mm, 1.9 mm, 1.4 mm and 1 mm for $\phi = 10$ mm, $\phi = 8$ mm $\phi = 6$ mm and $\phi = 4$ mm, respectively.

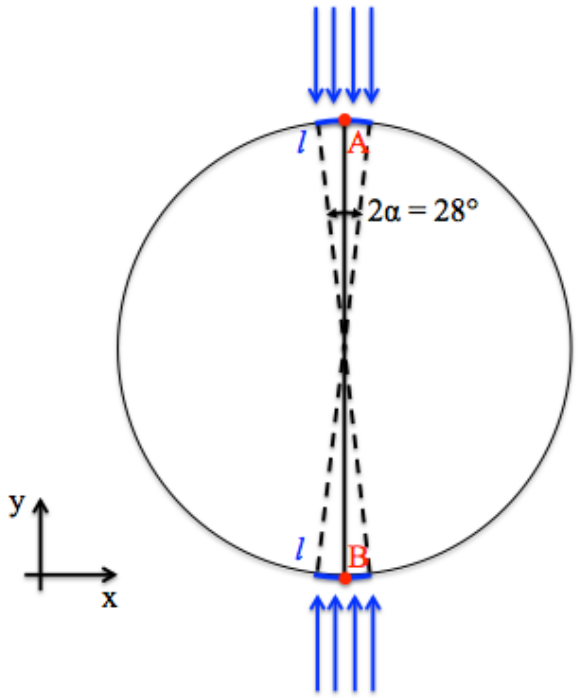

Figure 7: Boundary conditions for the simulation of the Bazilian test in COMSOL 3.5a.

2.4. Sensitivity analysis

The correction factor β_{ii-j} may change with respect to the elasticity coefficients. Therefore, a sensitivity analysis was performed for each specimen by varying the Young's moduli and Poisson's ratios by ± 10 % relative to the 'benchmark' values.

3. Results

3.1. Stress state in the loaded specimen

In this section we present the numerical results and in particular we discuss the stress field inside the specimen. As it is possible to observe in Fig. 8a and 8b, for a load per length unit $F = 1400$ N/mm (which is the same for each tested diameter), the compressive (σ_{yy}) and tensile (σ_{xx}) stresses are heterogeneously distributed. Their pattern is very similar to that of the isotropic case as reported in Wang et al. (2004) and specifically σ_{yy} and σ_{xx} are maximal along the loading surfaces and at the centre, respectively.

Actually, there exists a relationship between such stresses and the failure mechanism. In fact, as shown in Fig. 5, the crack is distinctly open at the centre of the disc ((x,y) = (0,0)) where the stress state is plane and given by

$$\underline{\underline{\sigma}} = \begin{pmatrix} \sigma_{xx} & 0 & 0 \\ 0 & \sigma_{yy} & 0 \\ 0 & 0 & 0 \end{pmatrix} \tag{4}$$

with $\sigma_{xx} = 55$ MPa and $\sigma_{yy} = -147$ MPa (blue line in Fig. 8d and 8b, respectively).

Let $\underline{n}$ and $\underline{t}$ be respectively the normal and the tangent vectors to the failure plane defined as

$$\underline{n} = \begin{pmatrix} cos\theta \\ sin\theta \\ 0 \end{pmatrix} \quad and \quad \underline{t} = \begin{pmatrix} -sin\theta \\ cos\theta \\ 0 \end{pmatrix} \tag{5}$$

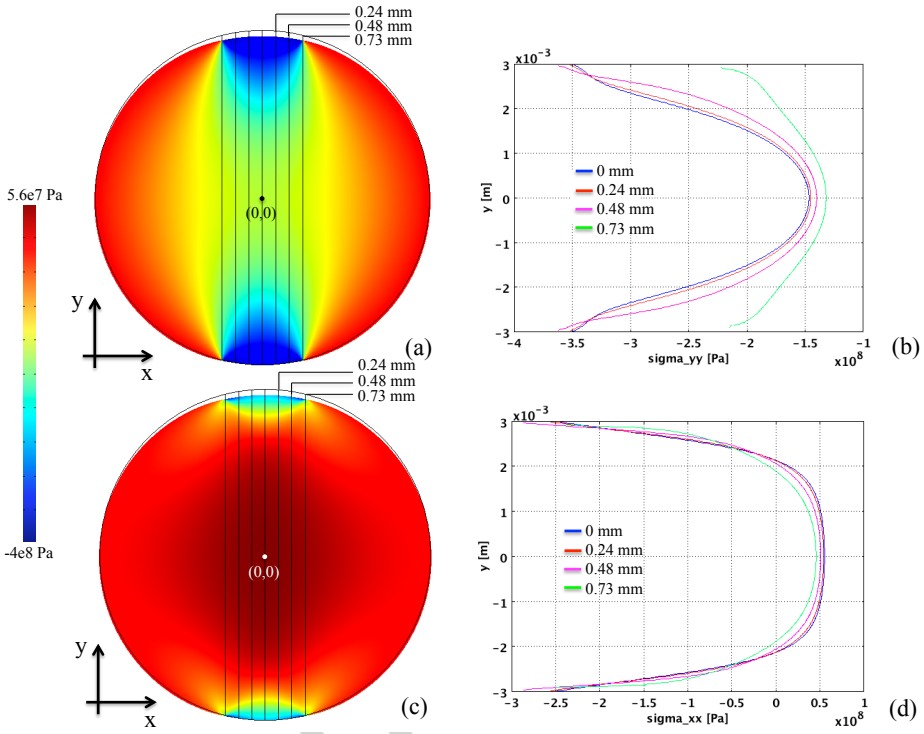

Figure 8: (a, c) Plot of σ_{yy} and σ_{xx}, respectively for a $x_1\_F_2$ specimen of diameter 6mm. (b, d) Outline of σ_{yy} and σ_{xx} respectively along the vertical diameter (blue line, $x = 0$) and along vertical lines placed at $x = 0.24$ mm (red line), $x = 0.48$ mm (purple line) and $x = 0.73$ mm (green line).

where θ is the angle between $\underline{n}$ and the $\underline{x}$ axis. Then, the normal (σ_n) and the shear (τ) stresses read

$$\sigma_n = \underline{n}^{tr}\,\underline{\underline{\sigma}}\,\underline{n} \tag{6}$$

$$\tau = \underline{t}^{tr}\,\underline{\underline{\sigma}}\,\underline{n} \tag{7}$$

with $\underline{n}^{tr}$ the transposition of $\underline{n}$.

It is interesting to evaluate the evolution of σ_n and τ for i) θ varying between 0° and 180° and ii) the axial coordinate x of the point of interest (x,y) varying between ±0.73 mm from the centre of the disc (Fig. 9).

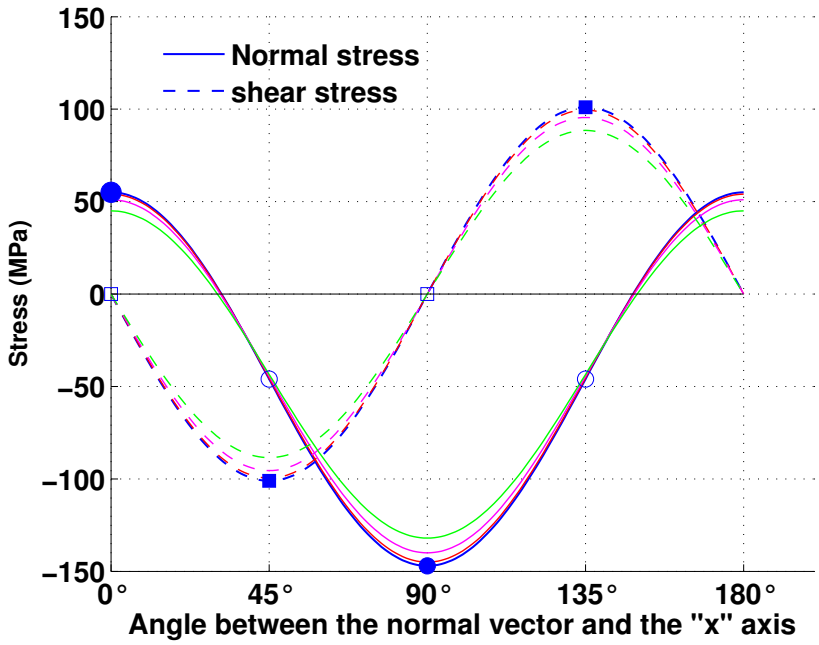

Figure 9: Normal and shear stress distribution at the centre and at 0.24 mm (red lines), 0.48 mm (purple lines) and 0.73 mm (green lines) from the centre along the x axis.

For $\theta = 0°$, we find $\sigma_n = 55$ MPa and no shear stress, while τ is maximal (± 100 MPa) for $\theta = 45°$ and 135°. Finally, for $\theta = 90°$, σ_n is equal to -147 MPa showing a compressive stress state (Fig. 9). It can be noticed that for

all these stresses, the maximal values are found at the centre of the disc (blue line in Fig. 8b, 8d, 9). For a brittle material, the failure plane is a useful parameter to evaluate the cracking mechanism and the corresponding stress. Here, failure is not activated at $\theta = 90°$ nor at $\theta = 45°$. On the contrary, the traction stress σ_{xx} is assumed to be responsible for the failure each time the crack occurs parallel to the loading axis.

The main objective of the numerical simulations was to evaluate the correction factor β_{ii-j} defined in Eq. [3], which is independent of the diameter ϕ of the disc. For an isotropic material, we found that such a coefficient is equal to 1 in the case of a concentrated load F_j and to 0.912 in the case of a distributed load as described in Sec. 2.3, which is very close to 0.92, the coefficient analytically calculated from Wang et al. (2004).

In order to use β_{ii-j} as a consistent indicator, the variation of the stress state must be low with respect to the cracking position. In Fig. 8b and 8d σ_{yy} and σ_{xx} respectively are plotted for a plane placed at $x = 0, 0.24, 0.48$ and 0.73 mm for a disc with a diameter of 6mm. We notice that if the crack occurs between ± 0.4 mm from the vertical axis of the disc, the maximum stress only varies by about ± 5.5 %. To keep such a low variability, the corresponding spatial tolerances for $\phi = 4, 8$ and 10 mm are $\pm 0.27, \pm 0.4$ and ± 0.67 mm, respectively. As an example, in Fig. 5, the diameter ϕ of the specimen is equal to 6 mm and the position of the crack is at 0.16 mm from the centre with an error of -1 % for the coefficient β_{ii-j}.

Finally, as mentioned in Sec. 2.4, a source of uncertainty for the correction factor β_{ii-j} is related to the variations of the elastic coefficients. According to the sensitivity analysis that has been carried out, the results for the four

loading cases are reported in Table 2.

Specimen	σ_{11}^f	σ_{22}^f	σ_{33}^f
$x_1\_F_2$	-	-	$\beta_{33-2} = 1.007 \pm 4\%$
$x_1\_F_3$	-	$\beta_{22-3} = 1.007 \pm 4\%$	-
$x_2\_F_1$	-	-	$\beta_{33-1} = 0.802 \pm 5\%$
$x_2\_F_3$	$\beta_{11-3} = 1.044 \pm 3.5\%$	-	-
$x_3\_F_1$	-	$\beta_{22-1} = 0.802 \pm 5\%$	-
$x_3\_F_2$	$\beta_{11-2} = 1.045 \pm 3.5\%$	-	-

Table 2: Results of the sensitivity analysis and values of correction factors β_{ii-j} for the four loading cases.

3.2. Experimental data

The experimental tests were exploited to assess the failure force as well as the crack direction, which must be vertical, and shape, which must be sharp-cut. Furthermore, by using the correction coefficients β_{ii-j} derived from the numerical analysis (Table 2), the values of the tensile failure stress were determined depending on the specimen diameter ϕ for each direction of failure stress tested σ_{11}^f, σ_{22}^f and σ_{33}^f (Fig. 10). Among the 29 tests carried out, 4 were stopped due to a crushing problem on the loading area (Sec. 2.2) and 4 presented a cracking mechanism outside the admissible region (Sec. 3.1) (hollow arrows in Fig. 10). For these specific cases, stress leading to failure was not usable as a value to rupture, but as an underestimation of the failure stress.

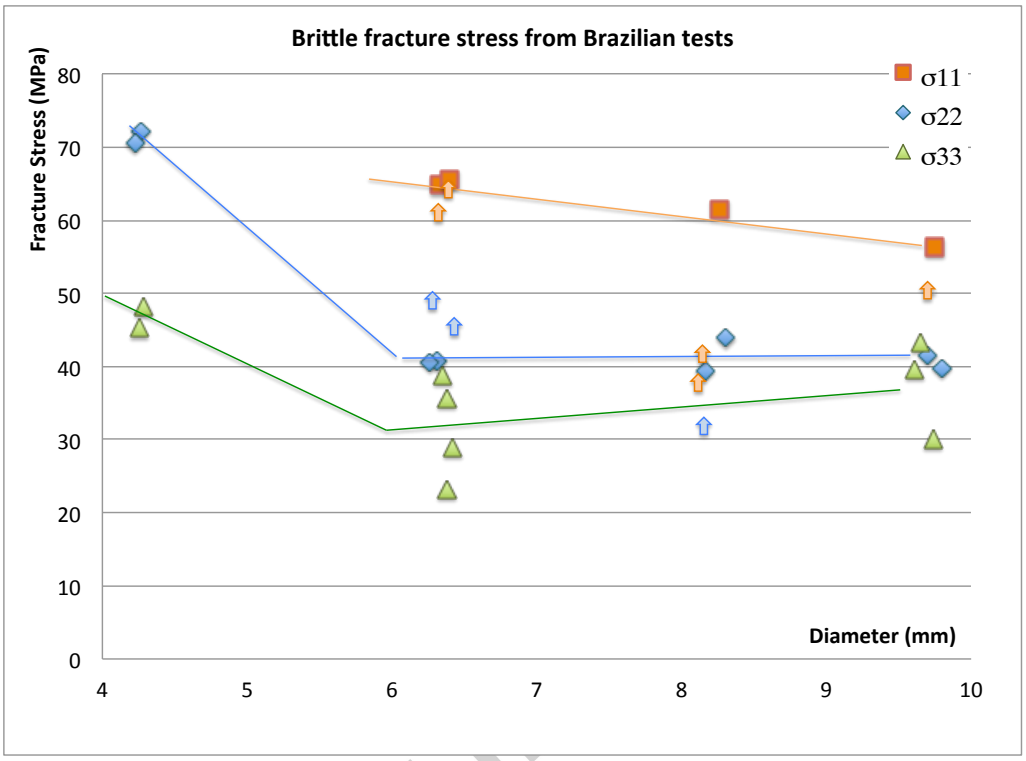

Figure 10: Maximum tensile stress versus diameter for three directions of loading.

The brittle strength is anisotropic for all the tested diameters and significantly higher along the axial direction. According to Fig. 10, the size of the specimen may influence the failure stress. For instance, for specimens with a diameter of 4 mm we observe an increase of the failure stresses. However, for $\phi = 6, 8$ and 10 mm, failure stresses are in the same order of magnitude along each direction and the average values are respectively equal to $\sigma_{11}^f = 62$ MPa, $\sigma_{22}^f = 41$ MPa and $\sigma_{33}^f = 34$ MPa.

As the traction stress σ_{xx} is not homogeneous within the sample (Fig. 8d), it may be of interest to identify a failure region for each specimen diameter

rather than simply determining the relationship between the failure stress and the sample dimensions. Thus, a rectangular area $S_{failure}$ of height $h_{failure}$ and width $e_{failure}$ can be defined for each diameter ϕ such that $0.9\,\sigma_{xx,max} < \sigma_{xx} < \sigma_{xx,max}$. We notice that the dimensions and consequently the area of the failure region decrease with the specimen diameter (Table 3).

Specimen diameter ϕ (mm)	4	6	8	10
Failure region height $h_{failure}$ (mm)	1.5	2.2	2.9	3.7
Failure region width $e_{failure}$ (mm)	0.8	1.2	1.6	2
Failure region area $S_{failure} = h \cdot e$ (mm^2)	1.2	2.64	4.64	7.4

Table 3: Values of the failure region area according to the specimen diameter ϕ.

4. Discussion

The Brazilian test is suitable for brittle materials only, but the experimental validation of the failure mechanism is very easy to achieve because the crack must be unique and in a vertical plane as described in Tavallali and Vervoort (2010). Additionally, if the ϕ/L ratio is controlled and optimised, the rare faulty tests may be attributed to machining or positioning defects. In the present work, although the bovine cortical bone we tested seemed rather young with a marked microstructure, the experimental dispersion was quite reasonable and the anisotropy of brittle fracture clearly appeared leading to a ratio $\sigma_{ii,max}/\sigma_{ii,min}$ of the order of 2.

For elastic isotropic materials, the fairly simple geometry of the specimen used for the Brazilian test allows the existence of analytical descriptions

of the stress field either for a concentrated or a distributed load. In this case, the analytical solution and our numerical simulation were in very good agreement. Specifically, for a concentrated load, the correction coefficient β_{ii-j} defined in Eq. [3] is exactly equal to 1, while for a distributed load as described in Sec. 2.3, β_{ii-j} is equal to 0.912.

For an anisotropic material such as cortical bone, the elastic coefficients deduced from Bernard et al. (2013) were used to run the numerical simulations for specimens of different diameters. We were able to determine the correction factors β_{ii-j} associated to each failure stress and we found that all the coefficients are between 0.802 and 1.05 or in a range of 0.92 $\pm$14 %. This results in a variation of the maximum stress of the order of 14 %. Furthermore, according to the sensitivity analysis we performed, the uncertainties on β_{ii-j} due to the variation of the elastic parameters are not higher than 5 %, which is quite low. Therefore, the coefficients can be directly used or, for better accuracy, recalculated after verification of the rigidity by, for example, an ultrasonic method.

The Brazilian test also allowed us to assess the scale influence on failure mechanism. The areas of the failure regions for the different specimens reported in Table 3 are very small for a tensile test on a brittle material, which results in failure stresses for specimens with a diameter of 4 mm higher than those for larger samples (Fig. 10). Previous works have focused on this specific aspect and have used either a Weibull distribution of the defect size (Fok et al., 2001) or a cohesive crack model (Guinea et al., 2000) to describe such a behaviour. In both cases, the size effect is attributed to an intrinsic length in correlation with the microstructure of the material, below which

the failure stress increases. This might also be the case for cortical bone. In fact, we can see that as the specimen diameter ϕ decreases, the dimensions $h_{failure}$ and $e_{failure}$ of the failure region decrease too (Table 3) and approach the dimensions of a portion of the cement line (Sec. 1.1), which may constitute a weakness for failure behaviour as mentioned in (Norman and Wang, 1997) (O'Brien et al., 2007) (MFeerick et al., 2013).

According to the previous remarks, it would be interesting to perform the Brazilian test on a large number of specimens within a range of small dimensions. In fact, this would allow to consistently investigate the scale influence and the statistical dispersion and to characterise a suitable nonlocal model to be adopted for numerical simulations.

5. Conclusion

In this paper we have proposed the Brazilian test as an alternative technique to investigate both the anisotropic strength and failure mechanism of cortical bone. In fact, although this test has rarely been employed in the field of bone biomechanics (Turner-Walker and Parry, 1995) (Turner-Walker, 2011) (Huang et al., 2012), it presents some interesting features. Firstly, it allows testing of brittle materials in traction through the use of a compressive load. Secondly, it allows to reduce the specimen dimensions down to those of the representative volume of the material. Then, for specific case of cortical bone it has been possible to assess the tensile failure along its three main axes and its anisotropy.

6. Bibliography

Akazawa, T., 1943. A new test method for evaluating internal stress due to compression of concrete: the splitting tension test. J. Japan. Soc. Civil. Eng. 19, 777–787. 8

Arcan, M., Hashin, Z., Voloshin, A., 1978. A method to produce uniform plane-stress states with applications to fiber-reinforced materials. Exp. Mech. 18 (141-146). 7

Arramon, Y. P., Mehrabadi, M. M., Martin, D. W., Cowin, S. C., 2000. A multidimensional anisotropic strength criterion based on a multidimensional anisotropic strength criterion based on kelvin modes. International Journal of Solids and Structures 37, 2915±2935. 4

Ascenzi, M.-G., Kawas, N. P., Lutz, A., Kardas, D., Nackenhorst, U., Keyak, J. H., 2012. Individual-specific multi-scale finite element simulation of cortical bone of human proximal femur. Journal of Computational Physics. 3

Ashman, R., Cowin, S., Buskirk, W. V., Rice, J., 1987. Elastic properties of cancellous bone: Measurement by an ultrasonic technique. J. Biomech. 17, 349–361. 5

Bernard, S., Grimal, Q., Laugier, P., 2013. Accurate measurement of cortical bone elasticity tensor with resonant ultrasound spectroscopy. Journal of the Mechanical behavior of biomedical materials 18, 12–19. 5, 15, 24

Carneiro, 1943. A new method to determine the tensile strength of concrete. In: Proceedings of the 5th meeting of the Brazilian Association for Technical Rules, 3d. section. 8

421 Currey, J. D., 2001. Bones: structure and mechanics. Princeton University
422 Press. 2

423 Doblare, M., Garcıa, J., Gomez, M., 2004. Modelling bone tissue fracture
424 and healing: a review. Engineering Fracture Mechanics 71, 1809–1840. 4

425 Exadaktylos, G., Kaklis, K., 2001. Applications of an explicit solution for the
426 transversely isotropic circular disc compressed diametrically. International
427 Journal of Rock Mechanics and Mining Sciences 38, 227–243. 13

428 Fok, S., Mitchell, B., Smart, J., Marsden, B., 2001. A numerical study on the
429 application of the weibull theory to brittle materials. Engineering Fracture
430 Mechanics 68, 1171–1179. 24

431 Funk, M., Litsky, A., 1998. Effect of cement modulus on the shear properties
432 of the bone-cement interface. Biomaterials 19, 1561–1567. 7

433 Guinea, G., Elices, M., Planas, J., 2000. Assessment of the tensile strength
434 through size effect curves. Engineering Fracture Mechanics 65, 189–207.
435 24

436 Hashin, Z., 1996. Finite thermoelastic fracture criterion with application to
437 laminate racking analysis. J. Mech. Phys. Solids 44 (7), 1129–1145. 4

438 Hoc, T., Henry, L., Verdier, M., Aubry, D., Sedel, L., meunier, A., 2006.
439 Effect of microstructure on the mechanical properties of haversian cortical
440 bone. Bone 38, 466–474. 5

441 Hondros, G., 1959. The evaluation of poisson's ratio and the modulus of
442 materials of a low tensile resistance by the brazilian (indirect tensile) test

with particular reference to concrete. Journal of applied science 10 (3), 243–268. 12, 13

Huang, S., L.S. Lin, A. F., Lin, C., 2012. Diametral compression test with composite disk for dentin bond strength measurement – finite element. Dent. Mater. 28, 1098–1104. 8, 25

Iosipescu, N., 1967. New accurate procedure for single shear testing of metals. J. Mater. 2, 537–566. 7

Li, S., Demirci, E., Silberschmidt, V. V., 2013. Variability and anisotropy of mechanical behavior of cortical bone in tension and compression. Journal of the Mechanical behavior of biomedical materials 21, 109–120. 8

MFeerick, E., Liu, X. C., McGarry, P., 2013. Anisotropic mode-dependent damage of cortical bone using the extended finite element method (xfem). Journal of the Mechanical behavior of biomedical materials 20, 77–89. 4, 25

Norman, T. L., Wang, Z., 1997. Microdamage of human cortical bone: Incidence and morphology in long bones. Bone 20 (4), 375–379. 4, 25

O'Brien, F. J., Taylor, D., Lee, T. C., 2007. Bone as a composite material: The role of osteons as barriers to crack growth in compact bone. International journal of fatigue 29, 1051–1056. 4, 25

Peltier, R., 1954. Theoretical investigation of the brazilian test. Rilem Bull 19, 26–69. 12

Puck, A., Schürmann, H., 1998. Failure analysis of FRP laminates by means of physically based phenomenological models. Composites Science and Technologiy 58, 1045–1067. 4

Reilly, D., Burnstein, A., 1974. The elastic modulus for bone. J. Biomech. 7, 271–275. 5

Reilly, D., Burstein, A., 1975. The elastic and ultimate properties of compact bone tissue. J. Biomech. 8, 393–405. 3, 4, 5, 6

Rho, J.-Y., Kuhn-Spearing, L., Zioupos, P., 1998. Mechanical properties and the hierarchical structure of bone. Medical Engineering and Physics 20, 92–102. 2, 3, 5

Sharma, N., Sehgal, D., Pandey, R., 2011. Studies on locational variation of shear properties in cortical bone with iosipescu shear test. Applied Mechanics and Materials 148-149 (276-281). 7

Tavallali, A., Vervoort, A., 2010. Behaviour of layered sandstone under brazilian test conditions: Layer orientation and shape effects. International Journal of Rock Mechanics and Mining Sciences 47, 313–322. 23

Turner-Walker, G., 2011. The mechanical properties of artificially aged bone: Probing the nature of the collagen–mineral bond. Palaeogeography, Palaeoclimatology, Palaeoecology 310, 17–22. 8, 25

Turner-Walker, G., Parry, T., 1995. The tensile strength of archaeological bone. Journal of Archaeological Science 22, 185–191. 2, 8, 25

485 Vashishth, D., 2007. Hierarchy of bone microdamage at multiple length
486 scales. International journal of fatigue 29 (6), 1024–1033. 2

487 Vayron, R., Barthel, E., mathieu, V., Soffer, E., Anagnostou, F., Haiat,
488 G., 2012. Nanoindentation measurements of biomechanical properties in
489 mature and newly formed bone tissue surrounding an implant. J. Biomech.
490 Eng. 134, 021007. 5

491 Wang, Q., Jia, X., Kou, S., Zhang, Z., Lindqvist, P.-A., 2004. The flattened
492 brazilian disc specimen used for testing elastic modulus, tensile strength
493 and fracture toughness of brittle rocks: analytical and numerical results.
494 International Journal of Rock Mechanics and Mining Sciences 41, 245–253.
495 12, 17, 20

496 Xavier, J., Diaquino, B., Morais, J., Pereira, F., 2013. Characterisation of
497 shear behaviour of bovine cortical bone by coupling the arcan test with
498 digital image correlation. Journal of the Mechanical behavior of biomedical
499 materials. 5